Journal Pre-proof

Using in vitro lipolysis and SPECT/CT in vivo imaging to understand oral absorption of fenofibrate from lipid-based drug delivery systems

Thuy Tran, Peter Bønløkke, Cristina Rodríguez-Rodríguez, Zeynab Nosrati, Pedro Luis Esquinas, Nrupa Borkar, Jakob Plum Christensen, Sophie Susanna Strindberg Andersen, Stoyan Karagiozov, Thomas Rades, Anette Müllertz, Katayoun Saatchi, Urs O. Häfeli

PII: S0168-3659(19)30681-9

DOI: https://doi.org/10.1016/j.jconrel.2019.11.024

Reference: COREL 10029

To appear in: *Journal of Controlled Release*

Received date: 19 August 2019

Revised date: 17 November 2019

Accepted date: 18 November 2019

Please cite this article as: T. Tran, P. Bønløkke, C. Rodríguez-Rodríguez, et al., Using in vitro lipolysis and SPECT/CT in vivo imaging to understand oral absorption of fenofibrate from lipid-based drug delivery systems, *Journal of Controlled Release* (2019), https://doi.org/10.1016/j.jconrel.2019.11.024

This is a PDF file of an article that has undergone enhancements after acceptance, such as the addition of a cover page and metadata, and formatting for readability, but it is not yet the definitive version of record. This version will undergo additional copyediting, typesetting and review before it is published in its final form, but we are providing this version to give early visibility of the article. Please note that, during the production process, errors may be discovered which could affect the content, and all legal disclaimers that apply to the journal pertain.

© 2019 Published by Elsevier.

Using *in vitro* lipolysis and SPECT/CT *in vivo* imaging to understand oral absorption of fenofibrate from lipid-based drug delivery systems

Thuy Tran [a], Peter Bønløkke [a], Cristina Rodríguez-Rodríguez [b,c,d], Zeynab Nosrati [b], Pedro Luis Esquinas [e], Nrupa Borkar [a], Jakob Plum Christensen [a], Sophie Susanna Strindberg Andersen [a], Stoyan Karagiozov [b], Thomas Rades [a], Anette Müllertz [a,e], Katayoun Saatchi [b]* and Urs O. Häfeli [b]**

[a] Department of Pharmacy, Faculty of Health and Medical Sciences, University of Copenhagen, 2100 Copenhagen, Denmark.

[b] Faculty of Pharmaceutical Sciences, University of British Columbia, Vancouver, BC V6T 1Z3, Canada.

[c] Department of Physics and Astronomy, University of British Columbia, Vancouver, BC V6T 1Z1, Canada.

[d] Medical Imaging Research Group, Department of Radiology, University of British Columbia, Vancouver, BC V5Z 1M9, Canada.

[e] Bioneer: FARMA, Faculty of Health and Medical Sciences, University of Copenhagen, 2100 Copenhagen, Denmark.

* Corresponding authors: anette.mullertz@sund.ku.dk, kathy.saatchi@ubc.ca, urs.hafeli@ubc.ca

Journal Pre-proof

ABSTRACT

Using lipid-based drug delivery systems (LbDDS) is an efficient strategy to enhance the low oral bioavailability of poorly water-soluble drugs. Here the oral absorption of fenofibrate (FF) from LbDDS in rats was investigated in pharmacokinetic, *in vitro* lipolysis, and SPECT/CT *in vivo* imaging studies. The investigated formulations were soybean oil solution (SBO), a mixture of soybean oil and monoacyl phosphatidylcholine (MAPC) (SBO-MAPC), self-nanoemulsifying drug delivery systems with and without MAPC (SNEDDS-MAPC and SNEDDS, respectively), and an aqueous suspension (SUSP) as a reference. Oral bioavailability of the LbDDS ranged from 27 to 35%. A two-step *in vitro* lipolysis model simulating rat gastro-intestinal digestion provided *in vitro* FF solubilisation data to understand oral absorption. During the *in vitro* lipolysis, most FF was undissolved for SUSP and distributed into the poorly dispersed oil phase for SBO. For the SNEDDS without MAPC, practically all FF solubilised into the aqueous phase during the dispersion and digestion. Adding MAPC to SBO enhanced the dispersion of the oil phase into the digestion media while adding MAPC to SNEDDS resulted in a distribution of 29% of FF into the oil phase at the beginning of *in vitro* lipolysis. FF distribution into both oil and aqueous phases explained the higher and prolonged oral absorption of LbDDS containing MAPC. To elucidate the relatively low bioavailability of all formulations, FF and triolein were labelled with ^{123}I and ^{125}I, respectively, to study the biodistribution of drug and lipid excipients in a dual isotope SPECT/CT *in vivo* imaging study. The concentration of radiolabeled drug as a function of time in the heart correlated to the plasma curves. A significant amount of radiolabeled drug and lipids (i.e., 28–59% and 24–60% of radiolabelled drug and lipids, respectively) was observed in the stomach at 24 h post administration, which can be linked to the low bioavailability of the formulations. The current study for the first time combined *in vitro* lipolysis and dual isotope *in vivo* imaging to find the root cause of different fenofibrate absorption profiles from LbDDS and an aqueous suspension.

KEYWORDS

Lipid-based drug delivery systems, monoacyl phosphatidylcholine, surfactant, SPECT/CT, *in vitro* lipolysis, pharmacokinetics, biodistribution, fenofibrate, dual radioisotope imaging

Journal Pre-proof

1. INTRODUCTION

Modern drug discovery programs have discovered a large number of poorly water-soluble drug candidates with low oral absorption [1]. To enable an effective oral delivery of these molecules, lipid-based formulations (LbDDS) including self-nanoemulsifying drug delivery systems (SNEDDS) have been used with success [2]. The use of natural surfactants has been investigated to reduce the content of synthetic surfactants, while maintaining the emulsification capacity and oral absorption enhancement facilitated by LbDDS [3, 4]. Previous studies on the use of monoacyl phosphatidylcholine (MAPC), which is a desirable natural surfactant, has clarified its effect on emulsion droplet sizes and colloidal structures formed during *in vitro* lipolysis, while understanding its effect on oral absorption is still a challenge [5].

In vitro lipolysis models has been used to predict and assess the capacity of LbDDS to enhance oral absorption [6]. During lipid digestion, the drug solubilisation capacity changes as digestion products are formed and the drug transfers from the original LbDDS into more polar and well-dispersed colloidal systems in the aqueous phase. Drug partitioning into the different phases formed during *in vitro* lipolysis (i.e., oil, aqueous or pellet phases) is thus commonly studied [6-9]. However, existing *in vitro* lipolysis models have been developed to simulate human digestion and thus might not predict the oral bioavailability of a drug in animals very well [10-14]. Therefore, the development of *in vitro* lipolysis models simulating animal digestion conditions is necessary to better predict *in vivo* drug absorption at preclinical phase.

Visualizing the *in vivo* biodistribution of drugs after oral administration can be an effective strategy to understand drug absorption and the interplay between drug and excipients before and after absorption. *In vivo* imaging has been used to investigate the passage of drug and excipients in the body, but mostly with magnetic-resonance-based non-quantitative methods, and rarely in the research field of oral LbDDS delivery [15]. As one of the most cutting-edge *in vivo* imaging techniques, single photon emission computed tomography (SPECT) combined with computed tomography (CT) can precisely quantify the amount of drug and lipid excipients distributed in each organ of a living animal [16-20]. For this purpose, drug and excipient are radiolabeled with two different isotopes that can then be detected at the same time, by separating out their distinct energy windows.

Journal Pre-proof

The objective of the current study is to understand the oral absorption of the lipophilic model drug fenofibrate (FF) from LbDDS and an aqueous suspension (used as a reference) in rats using *in vitro* lipolysis and SPECT/CT *in vivo* imaging. First, oral absorption of FF from the five formulations (i.e. four different LbDDS and the aqueous suspension) was evaluated in a pharmacokinetic study in rats. Then, the formulations were assessed using an *in vitro* lipolysis model simulating rat gastro-intestinal lipid digestion to understand the effect of digestion on oral absorption. Finally, the model drug FF and triolein were radiolabeled with ^{123}I and ^{125}I, respectively (Fig. 1). LbDDS with both ^{123}I-FF and ^{125}I-triolein were dosed orally to rats and dual-isotope SPECT/CT imaging was performed after administration and subsequently confirmed by a biodistribution study at 24 h to visualize the distribution of both the drug and the lipid excipients after oral administration. From *in vitro* lipolysis and SPEC/CT imaging studies, information on drug solubilisation in the gastro-intestinal tract and drug distribution in different organs is expected to provide an explanation for the varying drug absorption obtained from different formulations.

2. MATERIALS AND METHODS

2.1 Materials

Lipoid S LPC 80 (LPC) (from soybean, containing MAPC (81%) and phosphatidylcholine (PC) (13%) of C18:2 (48–56%), C16:0 (20–27%), C18:0 (5–8%), C18:1 (7–9%) fatty acid (FA)) and Lipoid S PC (from soybean, containing 98.0% PC) were kindly donated by Lipoid GmbH (Ludwigshafen, Germany). Kolliphor EL (polyoxyl 35 castor oil) (containing glycerol-polyethylene glycol (PEG) ricinoleate, FA esters of PEG, free PEG and ethoxylate glycerol) was kindly donated by BASF (Ludwigshafen, Germany). Maisine 35-1 (containing monoglycerides (MG) (33.5%), diglycerides (DG) (50.9%) and triglycerides (TG) (14.7%) predominantly of C18:1, C18:2 and C16:0 FA [21]) was kindly provided by Gattefossé (Saint-Priest, France). FF, hydroxypropyl methyl cellulose (HPMC), soybean oil (TG of mainly C18:2, C18:3, C18:1, C18:0 and C16:0 FA [22]), pancreatin from porcine pancreas (8 × United States Pharmacopeia (USP) specification activity), lipase from *Rhizopus oryzae* (~10 U/mg), bile bovine, tris(hydroxymethyl)aminomethane (Tris), maleic acid, and 4-bromophenyl-boronic acid (4-BPB) (≥ 95.0% pure) and organic solvents (including dichloromethane (DCM), methanol (MeOH) and ethanol (EtOH)), as well as Bu_6Sn_2 and $Pd(PPh_3)_4$ were purchased from Sigma-Aldrich (St. Louis, MO, USA). Sodium chloride was purchased from VWR (Søborg, Denmark). Sodium hydroxide (NaOH) pellets were obtained from Merck (Darmstadt, Germany). Water was purified using a SG Ultraclear water system

(SG Water GmbH, Barsbüttel, Germany). $Na^{123}I$ was obtained from Nordion (Vancouver, BC, Canada) and $Na^{125}I$ was obtained from American Radiolabeled Chemicals Inc. (St. Louis, MO, USA).

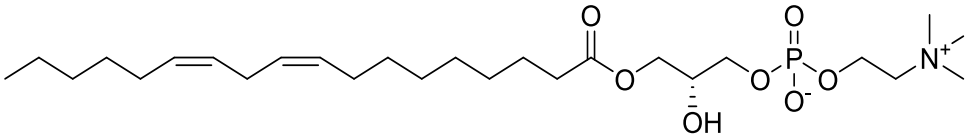

A1

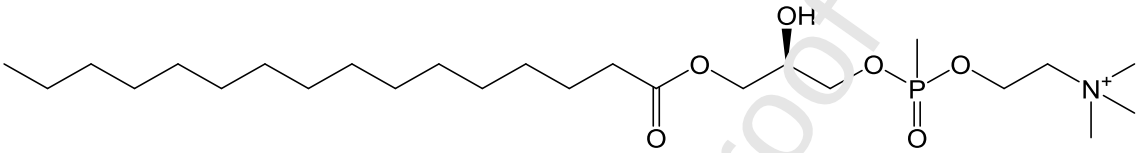

A2

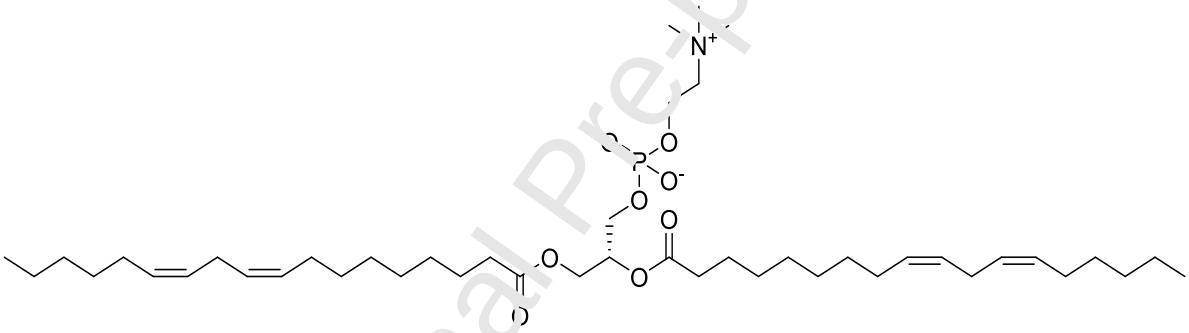

A3

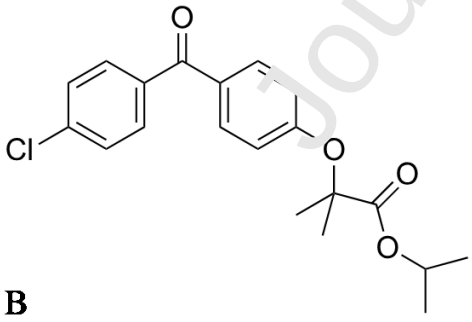

B

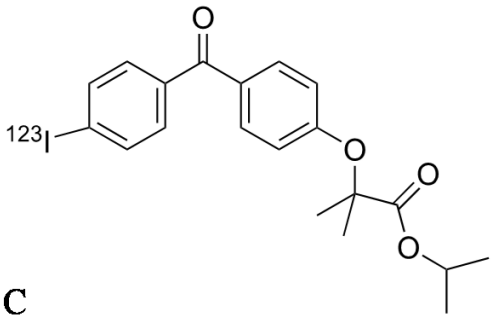

C

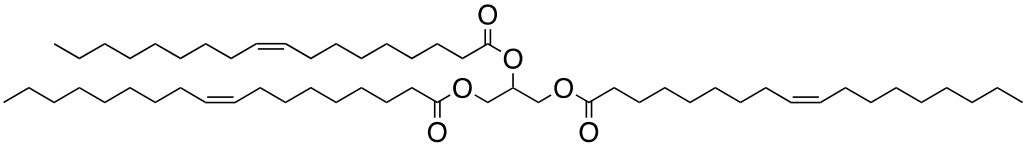

D

Journal Pre-proof

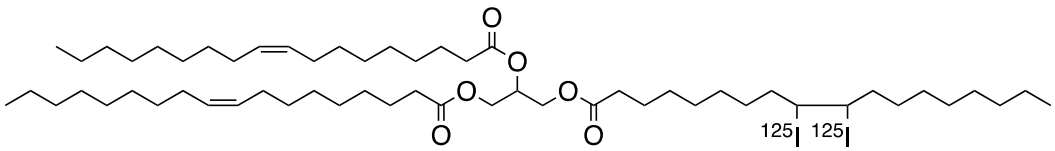

E

Fig. 1. Chemical structure of (A1, A2, A3) Lipoid S LPC 80 (MAPC (80%) and PC (13%) of C18:2 (48-56%), C16:0 (20-27%), C18:0 (5-8%), C18:1 (7-9%) FA), (B) FF, (C) ^{123}I-FF, (D) triolein, and (E) a potential radioiodinated structure for triolein (substitution can happen at any of the double bonds of triolein).

2.2. Methods

2.2.1. Preparation of formulations

The composition of the investigated LbDDS before adding FF is shown in Table 1. Maisine 35-1 was melted at 50 °C and homogenized before preparing SNEDDS and SNEDDS-MAPC. All LbDDS were prepared by weighing all excipients and FF into a glass vial to obtain a FF concentration of 35 mg/g followed by mixing with a magnetic bar for 5 h at 50 °C. The LbDDS were equilibrated overnight at room temperature before use. An aqueous suspension, designated as SUSP, was prepared by mixing FF in 0.5% HPMC solutions overnight at room temperature to obtain a FF concentration of 35 mg/mL.

Table 1. Composition of blank LbDDS.

Formulation	Composition (% w/w)			
	Soybean oil	Maisine 35-1	Kolliphor EL	Lipoid S LPC 80
SBO	100	-	-	-
SBO-MAPC	70	-	-	30
SNEDDS	20	20	60	-
SNEDDS-MAPC	20	20	30	30

2.2.2. *In vivo* pharmacokinetic study

The protocol used for the pharmacokinetic study was approved by the institutional ethics committee in accordance with Danish law regulating animal experiments and in compliance with EU directive 2010/63/EU and the NIH guidelines on animal welfare. Male Sprague-Dawley rats (315-372 g) were purchased from Charles River (Sulzfeld, Germany). Seven days prior to the experiment, the animals were acclimatized in standard housing conditions with bedding materials in each cage and maintained on standard feed with free access to

water. The animals were fasted by removing the food 12 h before the oral dosing of the formulations. Twenty-five rats in groups of five received one formulation each at the same dose of 35 mg/kg FF via oral gavage. The animals were allowed free access to water during the whole experiment and were provided standard feed at 6 h post administration. Blood samples (200 µL) were collected from the tail vein and transferred into 0.5 mL EDTA-coated tubes (BD, Franklin Lakes, NJ, USA) at 30 min and 1, 2, 3, 4, 6, 8, 10, and 24 h post administration. Plasma was taken by immediately centrifuging the blood samples for 15 min at 2,700 g and 4 °C (Spectrafuge, Labnet, NJ, USA), and stored at -20 °C until analysis. The animals were euthanized after the study. The bioanalytical procedure to analyse fenofibric acid level, the active drug released from fenofibrate, was previously described by Tran et al. [4].

2.2.3. *In vitro* lipolysis

The experimental setup comprised of two pH-stat apparatuses, two Titrando 842, two 804 Ti Stands, two 802 stirrers, two glass pH electrodes, two 800 Dosino dosing units, and two 10 mL autoburettes (Metrohm AG, Herisau, Switzerland) (Fig. 2). The amount of formulation containing 114 mg FF was dispersed for 2 min in 15 mL rat simulated gastric medium (Table 2) in a thermostated vessel maintained at 37 °C using a stirrer. The pH of the dispersion in gastric medium was manually adjusted to 4.0. After 4 min of gastric lipolysis, the transfer of the dispersed formulation was initiated into the intestinal vessel containing 15 mL rat simulated intestinal medium (Table 2) by a peristaltic pump at the rate of 0.93 mL/min. Porcine pancreatin extract was added to the intestinal medium when the formulation reached the intestinal vessel. After 10 min of intestinal lipolysis, the pump rate was reduced to 0.47 mL/min to simulate the kinetics of gastric emptying process in rats [23, 24]. The different applied pump rates allowed a half of the formulation dispersed in the gastric medium to be transferred into the intestinal vessel after 10 min of intestinal lipolysis, and after 30 min the rest of the formulation was completely transferred. The pH values of the gastric and intestinal media were maintained at 4.0 and 6.5 respectively, during the digestion by automatically adding NaOH to neutralize ionized fatty acid released. At 15, 30, 45, 60, 75, and 90 min of intestinal lipolysis, 3 mL samples were removed from the intestinal vessel and replaced by 3 mL of intestinal medium (Table 2) to simulate absorption. The withdrawn samples were subsequently analysed by HPLC as described in section 2.2.4. Bile salt concentration of gastric and intestinal medium during *in vitro* lipolysis is described in the **Supplementary Information** (Table S1).

Journal Pre-proof

Table 2. Composition of digestion medium used for the *in vitro* lipolysis model.

	Gastric medium	Intestinal medium
Initial total volume (mL)	15	15
Bile bovine (mM)	0.08	25.00 [25-27]
Phosphatidylcholine (mM)	0.02	2.75 [25, 28]
Sodium chloride (mM)	34.2	73.0
Calcium chloride (mM)	-	1.40
Tris maleate (mM)	2.0	2.0
pH	4.0 ± 0.1 [28]	6.5 ± 0.1 [28]
Lipase source	*Rhizopus oryzae*	Porcine pancreatin
Lipase activity (TBU/mL)	12.0 [29]	22.5 [30]

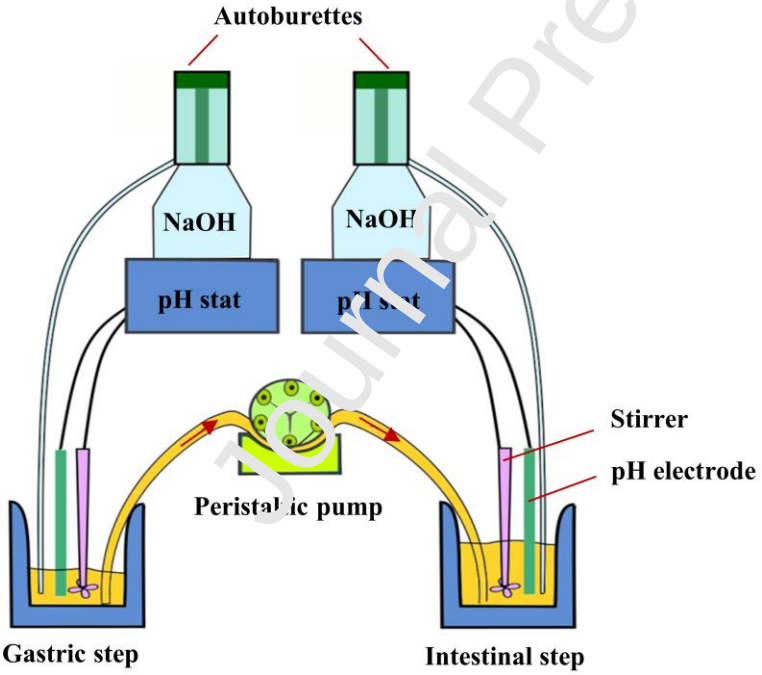

Fig. 2. *In vitro* lipolysis model simulating lipid digestion in rats. The formulation dispersed in simulated gastric medium is transferred to the intestinal medium using a peristaltic pump.

2.2.4. Determination of FF solubilisation during *in vitro* lipolysis

Two samples of one mL were taken at 0, 15, 30, 60, 75, and 90 min of intestinal digestion and immediately treated with lipolysis inhibitor (5 µL of 1.0 M 4-BPB (in MeOH) per mL of

sample). One sample was thoroughly mixed to determine the total amount of FF per mL. The other sample was centrifuged for 30 min at 19,100 g and 37 °C in a 5417R Eppendorf centrifuge (Hauppauge, NY, USA) to separate the oil, aqueous and pellet phases to determine the amount of FF distributed into the pellet and aqueous phases. The amount of FF was determined using a validated HPLC method previously described by Tran et al. [4].

2.2.5. Synthesis of ^{123}I-FF

^{123}I-FF was synthesised based on the method described by Breyer and co-workers (Fig. 3) [31]. The stannylation and radioiodination processes were performed as follows.

2.2.5.1. Synthesis of stannylated FF (Bu_3Sn-FF)

Bu_6Sn_2 (0.4 mL, 0.79 mmol) and $Pd(PPh_3)_4$ (99 mg) were successively added to a solution of I-FF (**1**) (Fig. 3) in anhydrous toluene (182 mg (0.4 mmol) in 6 mL) under nitrogen. The reaction mixture was heated at 80 °C for 18 h. The resulting mixture was cooled to room temperature and the dark solid formed was filtered through a silica pad and concentrated under reduced pressure. The residue was purified twice: (1) flash chromatography on silica using DCM/MeOH as an eluent in gradient to isolate the target product alongside with some impurities, (2) radial chromatography on a 1 mm plate using DCM/MeOH in gradient to obtain Bu_3S-FF (**2)** (122 mg, 49%) (Fig. 3). ^{1}H NMR (400 MHz, $CDCl_3$): δ 7.75 (d, 2H, J 8.9Hz), 7.65 (d, 2H, J 7.8Hz), 7.55 (d, 2H, J 8.1Hz), 6.84 (d, 2H, J 9.0Hz), 5.06 (sept, 1H, J 6.2Hz), 1.63 (s, 6H), 1.52 (m, 6H), 1.32 (m, 6H), 1.18 (d, 6H, J 6.2Hz), 1.07 (t, 6H, J 15.9, 7.6Hz), 0.87 (t, 9H, J 14.8, 7.5Hz). ESI-MS: *M/z* = 637 $[M + Na]^+$, 616 $[M + H]^+$.

2.2.5.2. Radioiodination process to form ^{123}I-FF

Bu_3S-FF (100 µL, 15 mg/mL EtOH) was injected into a Reacti-Vial™ containing $Na^{123}I$ (185 MBq). H_2O_2 (100 µL, 3% in HCl (1 M)) was added and the vial was mixed using an Eppendorf shaker at 900 rpm for 40 min. $NaHSO_3$ (150 µL, 0.1 M) was added and mixed to quench the reaction. The vial was vented with a filtered syringe, decapped and the contents neutralized with $NaHCO_3$ (150 µL, 0.1 M). The ^{123}I-FF was then extracted into 500 µL of DCM. The organic phase was transferred into a clean tube and DCM evaporated to leave ^{123}I-FF (70% labeling efficiency). Quality control was done by TLC against cold I-FF using hexane:MeOH:ethyl acetate mixture (at a ratio of 85:10:5) as eluent (R_f = 0.45).

Journal Pre-proof

^{1}H and ^{13}C NMR spectra were recorded at 400 and 100 MHz, respectively, on a Bruker AC 400 Ultrashield 10 spectrometer. Chemical shifts are expressed in ppm (δ scale). Standard abbreviations are used to report peak multiplicities. Coupling constants are reported in Hertz (Hz). Mass spectroscopy was performed on an AB SciexQTrap® 5500 hybrid linear ion-trap triple quadrupole mass spectrometer equipped with a Turbo Spray source (AB SCIEX, Concord, ON, Canada). The mass spectrometer was operated in positive or negative ionization mode and data were acquired using Analyst 1.5.2 software (SCIEX, Framingham, MA, USA) on a Microsoft Windows XP Professional operating platform.

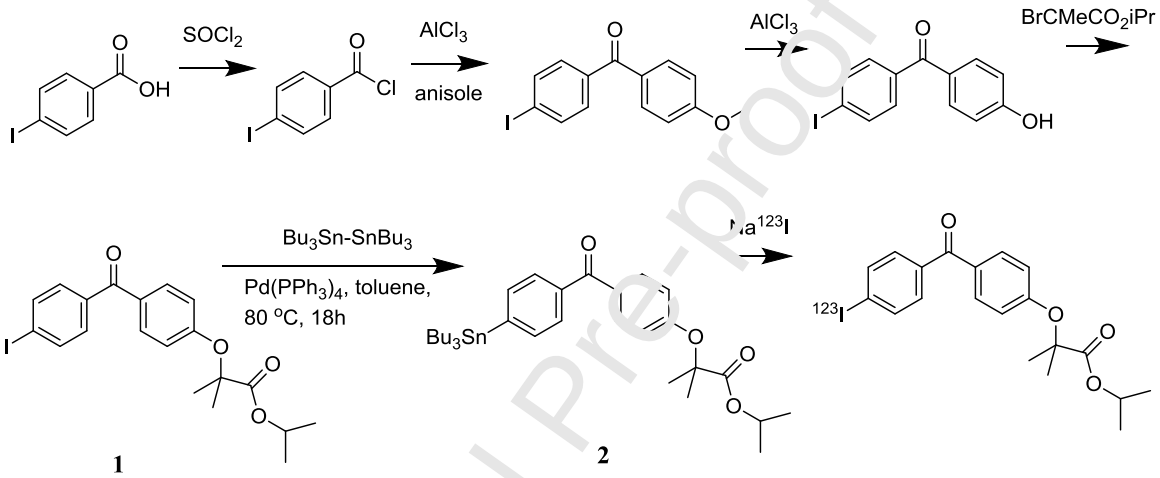

Fig. 3. Synthesis of radiolabeled ^{123}I-TFF. Adapted from Breyer et al. [31].

2.2.6. Synthesis of ^{125}I-triolein

^{125}I-triolein was synthesised in a hood approved for iodination based on the method described by Lubran et al. [32]. In brief, Na^{125}I (185 MBq in 500 µL NaOH (0.1 N)) was added to 3 mL ether in a 25 mL glass-stoppered cone shaped flask. KI (1 mL, 1 mg/mL), KIO_3 (0.5 mL, 2 mg/mL) and H_2SO_4 (200 µL, 2 N) were added in this order and the system was closed. The flask was shaken until all iodine was liberated into the etheric layer as indicated by the yellow colour. The colourless aqueous phase was then removed. To the organic layer 1 mL of freshly prepared chlorine dissolved in ether was added. To prepare this chlorine solution, $KMnO_4$ (50 mg) was placed in 5 mL diethyl ether under inert atmosphere and 500 µL of concentrated HCl was added to the mixture, followed by shaking the sealed system until the organic layer turned light yellow. The reaction flask was shaken until the turbid yellow mixture turned clear.

Journal Pre-proof

Triolein (500 µL) was dissolved in ether (1 mL) and mixed into the activated iodinating solution. The flask was left for 2 h with occasional stirring. The reaction was quenched by adding 7 mL of iodide thiosulphate solution which was made by mixing equal amounts of a 5% w/v KI and a 5% w/v $Na_2S_2O_4$ solution. The aqueous phase was removed and the organic phase washed twice with the same solvent, followed by three washes with water. The ether was evaporated to leave the ^{125}I-radiolabeled oil (15% labeling efficiency).

2.2.7. Biodistribution study

2.2.7.1. SPECT/CT imaging

2.2.7.1.1. Animal experiment procedure for SPECT/CT imaging

The study was performed in accordance with the Animal Care Committee of the University of British Columbia under the approved protocol A16-0150 and the NIH guidelines on animal welfare. Fifteen male Sprague-Dawley rats (Charles River, Canada) were randomly arranged in five groups of three rats, each group received one formulation via oral gavage. The fasting and dosing protocol of the biodistribution study was similar to the pharmacokinetic study (section 2.2.4) except that no blood samples were taken from the living animal and LbDDS was prepared with radioactive ^{123}I-FF and ^{125}I-triolein. ^{123}I-FF and ^{125}I-triolein were mixed with LbDDS and ^{123}I-FF was mixed with SUSP overnight using an Eppendorf Thermomixer R at the rate of 900 rpm at room temperature. Between 11.0–48.4 MBq of ^{123}I-FF and 4.3–32.3 MBq of ^{125}I-triolein was administered to each rat.

During the SPECT/CT imaging, the rats were anaesthetized using isoflurane (1–3% for maintenance, up to 5% for induction) in oxygen from a precision vaporizer and received a subcutaneous injection of lactated Ringer's solution (6 mL per hour of imaging) for hydration prior to the SPECT/CT imaging scan. The SPECT/CT imaging was performed on a VECTor/CT preclinical small animal scanner (MILabs, Utrecht, The Netherlands). Respiratory rate and body temperature of the animals were monitored constantly during the scans while isoflurane dose and bed temperature were accordingly adjusted. All animals recovered after each scan. The animals were euthanized by CO_2 after the final scan at 24 h post administration before cardiac puncture blood sampling and tissue collection.

2.2.7.1.2. Dual-isotope SPECT/CT parameters and image reconstruction

The whole-body SPECT data from ^{123}I and ^{125}I were simultaneously acquired in list-mode on a VECTor/CT scanner equipped with an ultra-high resolution rat and mouse (UHRRM)

Journal Pre-proof

multi-pinhole collimator [33]. Dynamic whole-body scans over 1 h (3 frames, 20 min/frame) were acquired at 30 min and 5 h after the oral administration to obtain details on passage of the drug and lipids every 20 min. For the results graphed in Figures 6-8, only the first frames were used of the 30 min and 5 h time points. Static one-hour scans were performed at 10 and 24 h after oral administration of the formulation to provide high quality images when the activity of ^{123}I decreases. Following each SPECT acquisition, a CT scan was performed to obtain anatomical information and correct the imaging data for photon attenuation to obtain fully quantitative images.

The list-mode data were used to generate projection images corresponding to the main photopeaks of ^{123}I and ^{125}I. For ^{123}I, a photopeak energy window was set at 160 keV (20% width, 144 keV–176 keV); two scatter windows (10% width) were set on each side of the photopeak (ranging from 126–144 keV and 176–192 keV for the lower and upper scatter windows, respectively). The ^{123}I projection data was reconstructed using a pixel-based OSEM method (16 subsets and 10 iterations) [34] with CT-based attenuation [35] and triple-energy window (TEW) scatter corrections [36]. The counts in the reconstructed image (referred to as $R_{160\ keV}$) were converted into units of activity concentration (in MBq/mL) by applying a phantom-based calibration factor [35, 37].

Since the ^{125}I photopeak at 25 keV overlaps with one of the photopeaks from ^{123}I, a method to remove the ^{123}I signal from the ^{125}I photopeak was developed to estimate the ^{125}I *in vivo* biodistribution using SPECT/CT. The method was divided into three steps. First, the parameter k that represents the ratio of reconstructed photopeak signals of ^{123}I at 25 keV and ^{123}I at 160 keV was estimated using a uniform phantom filled with ^{123}I and scanned with VECTor. The parameter k is independent of the attenuation and scattering conditions as it was determined from quantitative reconstructed images (i.e., images with attenuation and scatter corrections). Second, an image was reconstructed from the corresponding animal data using a photopeak centered at 25 keV (100% width, 12.5 – 37.5 keV) with triple-energy window scatter (scatter windows ranging from 7.5 - 12.5 keV and 37.5 - 42.5 keV for the lower and upper windows, respectively) and attenuation corrections using POSEM (16 subsets, 10 iterations). The resulting image (referred to as $R_{125+123}$) corresponds to the biodistribution image from both the ^{125}I and the ^{123}I X-ray photopeaks. Finally, the reconstructed ^{125}I biodistribution (R_{125}) was estimated by applying the following expression to the $R_{125+123}$ and the R_{160} images on a voxel by voxel basis:

Journal Pre-proof

$$R_{125}\ [counts/voxel] = R_{125+123}[counts/voxel] - k \times R_{160\ keV}\ [counts/voxel] \quad \text{(Eq. 1)}$$

The biodistribution of radioactivity was calculated based on SPECT/CT images and presented as standardized uptake values (SUV) (Eq. 2).

$$SUV\ [g/mL] = \frac{Concentration\ in\ volume\ of\ interest\ [MBq/mL]}{Injected\ dose\ [MBq]} \times Body\ weight\ [g] \quad \text{(Eq. 2)}$$

The animal body weight and injected dose were taken into account when normalizing SUV in each organ. This allows a direct comparison of different radioisotope distributions, such as in our case ^{123}I and ^{125}I, without further calculations. Further details regarding the dual-imaging with the two iodine radioisotopes were described by Nosrati et al. [38].

2.2.7.2. Biodistribution study using gamma counter measurement after animal euthanasia

After animal euthanasia at 25 h post administration, blood samples were immediately collected by cardiac puncture and animal organs (stomach, intestine, liver, thyroid, thymus, and bladder) removed from the body. The stomach content and tissue were separated and all organ tissues carefully divided. The radioactivity of the samples was measured using a Sodium-Iodide (NaI) Packard Cobra II auto-gamma counter (Canberra-Packard Canada Ltd, Mississauga, ON, Canada). The biodistribution of ^{123}I and ^{125}I per organ is presented as percent of injected dose (%ID) (Eq. 3).

$$\%ID = \frac{Measured\ organ\ activity\ (based\ on\ \gamma\text{-}counter\ measurement\ )\ [MBq]}{Total\ activity\ given\ to\ the\ rat\ (based\ on\ imaging\ analysis)\ [MBq]} \times 100 \quad \text{(Eq. 3)}$$

2.2.8. Data and statistical analysis

The pharmacokinetic profiles of SNEDDS are presented as fenofibric acid concentration in plasma (µg/mL) vs. time (h). The corresponding area under the curve (AUC) and elimination half-life were calculated based on non-compartmental analysis using Pharsight Phoenix® WinNonlin® 6.4 software (Certara, Mountain View, CA, USA). Statistical comparisons of the data were performed with one-way ANOVA followed by the Tukey mean comparison test (significant level $\alpha = 0.05$) using OriginPro 9.1 software (Origin Corporation, Northampton,

MA, USA). Pharmacokinetic data are presented as the mean ± standard error of the mean (SEM) (n = 5). All other data are presented as the mean ± standard deviation (SD) (n = 3).

3. RESULTS AND DISCUSSION

3.1. *In vivo* pharmacokinetic study in rats

The oral absorption of FF from the LbDDS and SUSP (Table 1) were assessed in a pharmacokinetic study in rats (Fig. 4). The corresponding pharmacokinetic parameters are summarized in Table 3. The absolute bioavailability of the five formulations ranged from 24 to 35% (Table 3), calculated based on the data obtained after injecting intravenously a 10 mg/mL FF nanoemulsion [39]. Among the five formulations, SUSP exhibited the lowest $AUC_{0–6\ h}$, $AUC_{0–24\ h}$ and C_{max} and the longest T_{max} (Table 3), corresponding to the slowest and lowest drug absorption. Among the four LbDDS, the C_{max} values of LbDDS containing surfactants (i.e., SBO-MAPC, SNEDDS, and SNEDDS-MAPC) were significantly higher than SUSP, while there was no significant difference between SBO and SUSP. Drug plasma concentration during the first 2 h post administration was ranked as follows: SNEDDS > SNEDDS-MAPC > SBO-MAPC > SBO > SUSP. The drug plasma concentration for SNEDDS increased fast before reaching a high C_{max} value and then rapidly decreased (Fig. 4). Compared to SNEDDS, the drug plasma concentration of SBO-MAPC and SNEDDS-MAPC decreased more slowly after reaching C_{max}. As a result, SBO-MAPC, SNEDDS-MAPC, and SNEDDS exhibited significantly higher $AUC_{0–6\ h}$ values than SUSP, while only SBO-MAPC and SNEDDS-MAPC did so for $AUC_{0–24\ h}$ (Table 3).

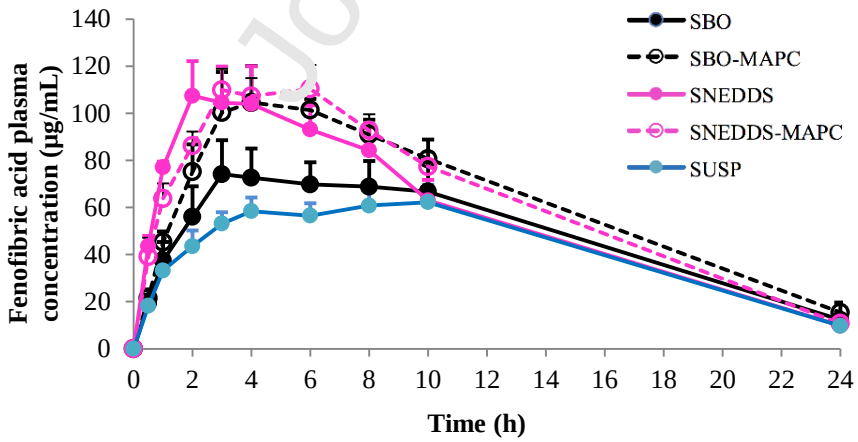

Fig. 4. Plasma concentration of fenofibric acid over 24 h following oral administration of the five formulations. The data are presented as mean + SEM (n = 5).

Table 3. Pharmacokinetic parameters of fenofibric acid following oral administration of the five formulations. The data are presented as mean ± SEM (n = 5).

Formulations	SBO	SBO-MAPC	SNEDDS	SNEDDS-MAPC	SUSP
$AUC_{0\text{-}6\ h}$(μg×h/mL)	347 ± 59	478 ± 58[a]	540 ± 58[b]	535 ± 21[c]	266 ± 13[a,b,c]
$AUC_{0\text{-}24\ h}$(μg×h/mL)	1173 ± 164	1515 ± 53[a]	1374 ± 114	1524 ± 72[b]	1025 ± 90[a,b]
C_{max} (μg/mL)	90 ± 11	124 ± 5[a]	122 ± 15[b]	125 ± 7[c]	68 ± 7[a,b,c]
T_{max} (h)	5.8 ± 1.7	5.0 ± 0.9	5.0 ± 1.3	4.4 ± 0.7[a]	9.2 ± 0.5[a]
$T_{1/2}$ (h)	5.9 ± 0.3	6.2 ± 1.1	5.3 ± 0.3	5.1 ± 0.3	5.3 ± 0.3
Absolute bioavailability *	27 ± 4	35 ± 1	32 ± 3	35 ± 2	24 ± 2

[a,b,c] Same superscript indicates significant differences in $AUC_{0\text{-}6\ h}$, $AUC_{0\text{-}24\ h}$, C_{max}, T_{max} or $T_{1/2}$ between the formulations (with $p < 0.05$)

* Absolute bioavailability was calculated based on the intravenous injection of 10 mg/mL FF nanoemulsion [39]

3.2. *In vitro* lipolysis

The dispersion and digestion of the formulations and drug solubilisation in simulated gastro-intestinal media was studied in the *in vitro* lipolysis model (Fig. 5) to understand FF oral absorption from the five formulations. The emulsification of LbDDS upon dispersion was visually observed and the solubilisation of FF in digested formulations was analysed at several time points. While most FF was solubilised in either the oil phase or the aqueous phase during 90 min of digestion of LbDDS (97–98% for SBO, SBO-MAPC, and SNEDDS and 91% for SNEDDS-MAPC), less than 3% of the drug was solubilised in the case of SUSP. This explained the enhanced rate and extent of absorption from all LbDDS compared to SUSP. During dispersion and digestion in the gastric and subsequently the intestinal medium, SBO formed an unstable coarse emulsion of which two phases rapidly separated when stopping agitation. LbDDS containing surfactants, i.e., SBO-MAPC, SNEDDS, and SNEDDS-MAPC, formed more stable colloidal systems in both gastric and intestinal media than SBO, which related to faster FF absorption from LbDDS containing surfactants compared to SBO.

During the *in vitro* intestinal digestion, the distribution of FF into the oil and aqueous phases are different between the four LbDDS (Fig. 4). FF concentration in the aqueous phase during 90 min of *in vitro* lipolysis can be ranked as: SNEDDS > SNEDDS-MAPC > SBO-MAPC ≈ SBO > SUSP (Fig. 5), similar as the ranking for drug plasma concentration during the first 2h

post administration (Fig. 4). Although similar amount of FF distributed into the oil phase of SBO-MAPC and SBO, the oil phase of SBO-MAPC emulsified much better than SBO in the simulated digestion media. Thus, the *in vivo* absorption rate of the formulations could be related to not only drug solubilisation but also emulsification capacity of the LbDDS.

Similar trends were found between the *in vitro* lipolysis and the pharmacokinetic study explaining the difference of C_{max}, T_{max}, and AUC values between formulations. With poor emulsification capacity and the high fraction of drug distributing into the oil phase, SBO exhibited low C_{max} and $AUC_{0\text{-}24\ h}$ values, or a low, but prolonged, oral absorption in rats (Fig. 4) compared to the other formulations. Incorporating MAPC into SBO enhanced the emulsification and drug concentration in the aqueous phase during dispersion and digestion, so that higher AUC and C_{max} were obtained corresponding to enhanced rate and extent of absorption. The presence of MAPC in SBO-MAPC and SNEDDS-MAPC allowed for a balance between drug distributed into aqueous and oil phases, which were well-emulsified, to obtain high drug plasma concentration, which increased faster than from SBO and more prolonged than from SNEDDS, and therefore resulted in high $AUC_{0\text{-}24\ h}$ value.

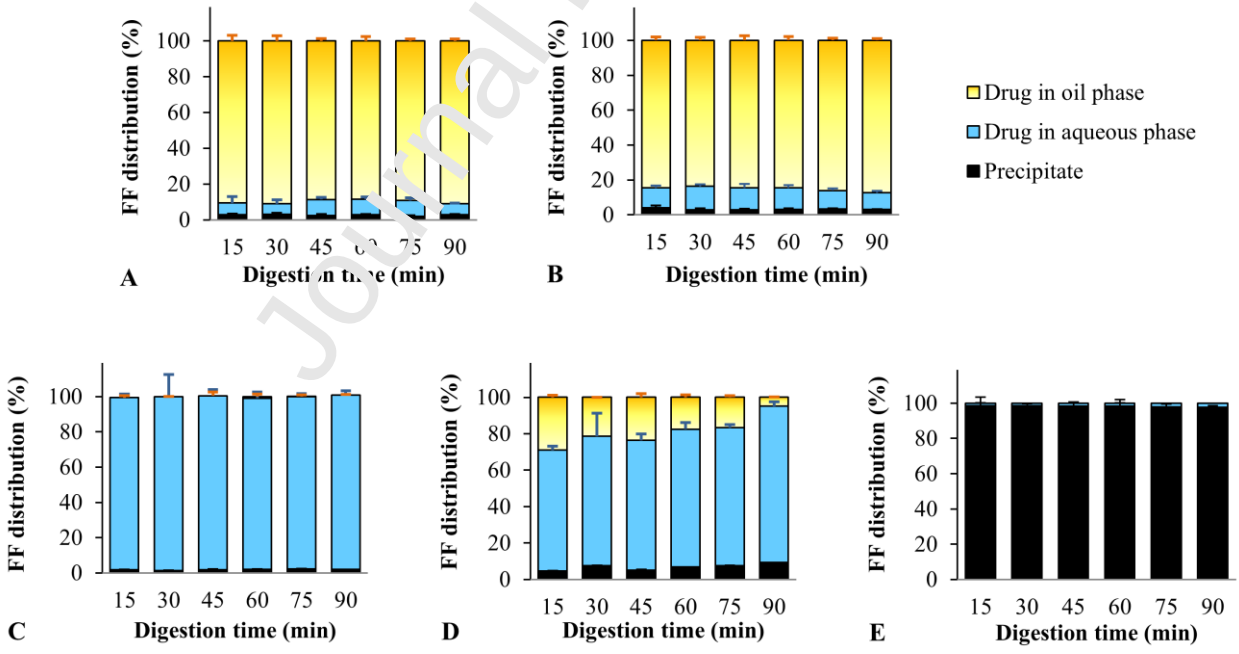

Fig. 5. Distribution of FF into the oil, aqueous and pellet phases in the intestinal phase during 90 min of *in vitro* lipolysis simulating rat conditions of (A) SBO, (B) SBO-MAPC, (C) SNEDDS, (D) SNEDDS-MAPC and (E) SUSP. The data are presented as mean + SD (n = 3).

3.3. Biodistribution study

3.3.1. SPECT/CT imaging

In vitro lipolysis explained the differences in terms of rate and extent of oral drug absorption when comparing formulations, but cannot explain the low absolute bioavailability of all formulations. The biodistribution of drug and lipids by using SPECT/CT imaging, as a non-invasive approach, was investigated with this objective. ^{123}I-FF and ^{125}I-triolein were used to label the drug and the lipid excipients, respectively. The biodistribution of drug and excipients can be obtained independently in the same animal during 24 h post administration, and thereby provide information on their passage through the gastro-intestinal tract and after being absorbed. New methods of radiolabelling fenofibrate and lipid excipients were investigated and acceptable yields of the iodination with ^{123}I (approximately 70% labelling efficiency for ^{123}I-FF) and ^{125}I (approximately 15% labelling efficiency for ^{125}I-triolein) were obtained. The high stability of radiolabeled ^{123}I-FF was confirmed in human serum by Breyer et al. [31]. ^{123}I-FF was shown to convert completely to radiolabeled fenofibric acid in homogenized mouse liver [31]. Both radioisotopes could be detected and quantified at acceptable statistics during 24 h after oral administration to rats.

Similarly to the FF metabolism [40, 41], the ester bond of ^{123}I-FF is expected to be hydrolysed to ^{123}I-fenofibric acid, which is metabolised in the liver to form ^{123}I-labeled glucuronide metabolites. A biodistribution study of ^{123}I-FF in mice after intravenous injection showed that most of the drug was accumulated in the liver, the target organ of FF or fenofibric acid, between 5 min and 6 h post administration [31]. Based on the metabolism of triolein [42], ^{125}I-triolein is suggested to form ^{125}I-oleic acid and ^{125}I-monooleate during the digestion, which both are absorbed into the enterocytes and delivered to the lymph and systemic blood as triglycerides in ^{125}I-chylomicrons. Fig. 6 shows SBO containing ^{123}I-FF/^{125}I-triolein as representative dynamic SPECT/CT images for the five formulations at 30 min and 5, 9.5 and 24 h post administration. The biodistribution of ^{123}I and ^{125}I indicates the biodistribution of the drug and lipids following oral administration.

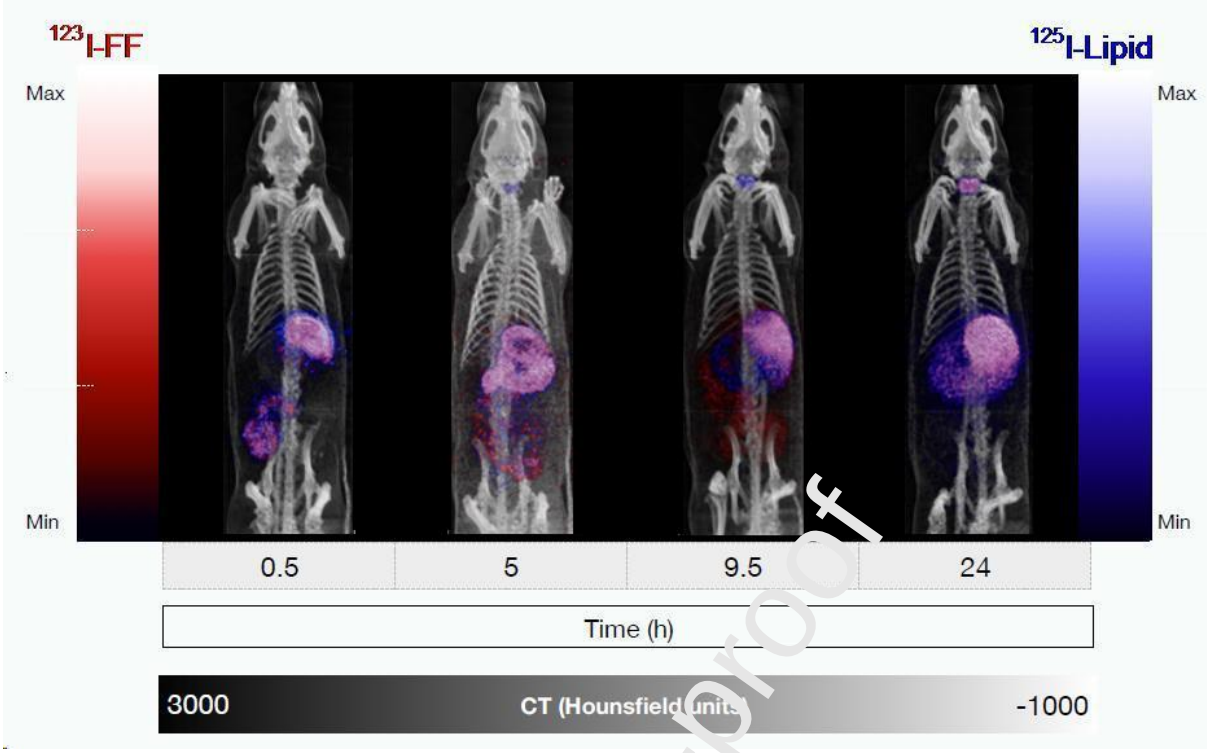

Fig. 6. Three-dimensional (3D) volume-rendered SPECT/CT images of radiolabeled drug (in red) and radiolabeled lipids (in blue) distributed in rats at 30 min, 5 h, 9.5 h, and 24 h after oral administration of SBO containing ^{123}I-FF/^{125}I-triolein. Regions where both radiolabeled drug and lipids reside are in pink. The SBO system is shown as a representative example of the investigated LbDDS, as activity distributions (see Figures 7 and 8) were not statistically different. 3D SPECT/CT images taken after oral administration of other formulations are mentioned in **Supplementary Information** (Figures S1-S4).

Based on the SPECT/CT image analysis, the movement of the radiolabelled drug and lipid excipient to and through the different organs could be followed over 24 h and is quantitatively shown in Fig. 7.

Journal Pre-proof

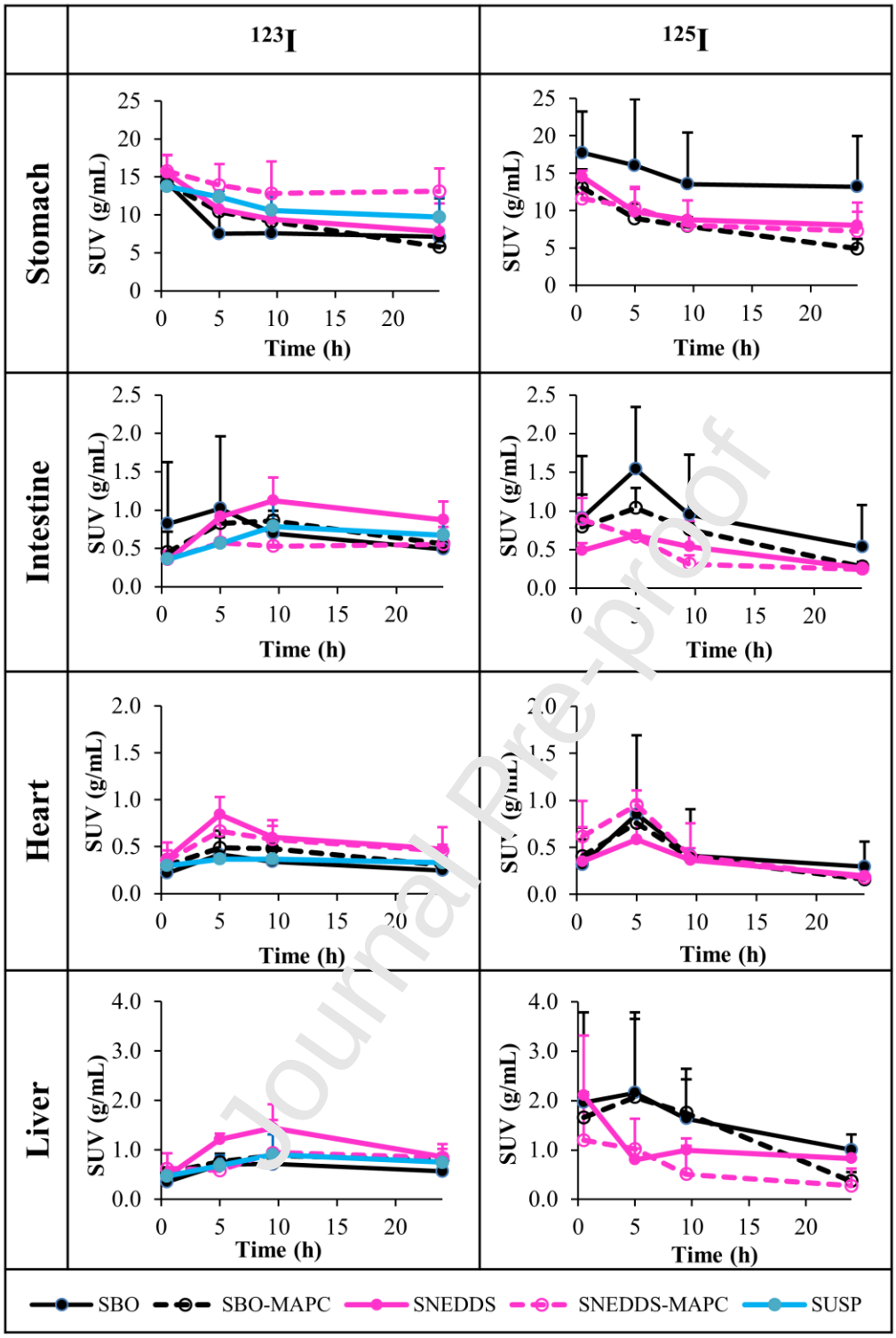

Fig. 7. Standardized uptake value (SUV) of (left) radiolabeled drug and (right) radiolabeled lipids at 30 min to 24 h after oral administration in rats in stomach, intestine, heart, and liver based on SPECT/CT images. The data are presented as mean + SD (n = 2–3).

SPECT/CT images show that both radiolabeled drug and lipids were found in the stomach and the intestine at 30 min after oral administration (Fig. 6), and then slowly moved

through the gastro-intestinal tract. The activities of ^{123}I and ^{125}I in the stomach, intestine, heart and liver were calculated from the SPECT/CT images and the previously performed phantom studies and calibration curves [38, 43] (Fig. 7).

Given in percentage of the administered dose, 56–71% of radiolabelled drug and 54–83% of radiolabelled lipids were found in the stomach 30 min after oral gavage, while between 4–9% of radiolabeled drug and 5–10% of radiolabeled lipid were found in the entire intestine (Fig. 8). As shown in Fig. 7, the amount of radioactivity from both isotopes in the stomach decreased over time with a faster gastric clearance rate during the first 9.5 h and slower clearance from 9.5–24 h post administration. At 24 h, significant radioactivity from both isotopes remained in the stomach, i.e., 28–59% of radiolabeled drug and 24–60% of radiolabeled lipid (Fig. 8). 5–9% of radiolabeled drug and 3% of radiolabeled lipid, was found in the intestine at the 24 h time point. The AUC values of SUV of radiolabeled drug and lipid over 24 h in the stomach and entire intestine are similar for the five formulations (Fig. 7).

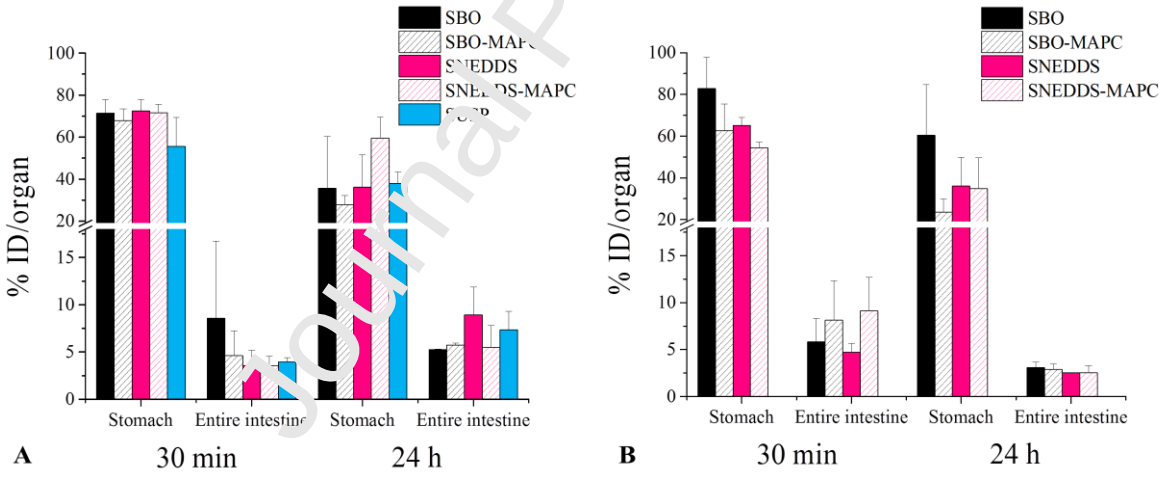

Fig. 8. Percentage of (A) radiolabeled drug and (B) radiolabeled lipids compared to injected dose (ID) in stomach and intestine at 30 min and 24 h after oral administration based on SPECT/CT image analysis. The data are presented as mean + SD (n = 2–3).

The direct equivalent of measuring blood drug concentrations in conventional pharmacokinetic studies is to choose the heart as the organ of interest in SPECT/CT studies and follow its radioactivity intensity. The SUV profile reflects mostly the heart's blood volume and allows for easy concentration calculations. In this study, both the ^{123}I

and the ^{125}I showed a maximum SUV in the heart at 5 h post administration (Fig. 7), which correlates well with the T_{max} in the pharmacokinetic study (Fig. 5). SUSP and SBO exhibited the lowest uptake of radiolabeled drug in the heart in the imaging study, similarly to their lowest mean drug plasma concentration versus time profile in the pharmacokinetic study. For SNEDDS, the high level found in the heart correlates with the high uptake in the liver, both of which may relate to the fast drug absorption seen in the pharmacokinetic study. In the pharmacokinetic study, SNEDDS did not perform significantly better than SBO and SUSP; but the drug uptake profiles in the heart showed that only SNEDDS exhibited significantly higher AUC compared to SBO and SUSP (Fig. 7). The difference between the imaging and the pharmacokinetic study is likely due to the lower number of time points during the imaging. Specifically, only four time points were allowed during 24 h because the duration of total anaesthesia was limited to ensure animal well-being. The activities could thus not be measured between 3-6 h, which did not allow to demonstrate and confirm the prolonged high drug plasma concentrations from SBO-MAPC and SNEDDS-MAPC in the pharmacokinetic study.

Interestingly, the SUV versus time profile of radiolabeled drug and lipid found in the heart were similar to the SUV profile in the intestine. The absorption of the two radiolabeled compounds seemed proportional to the amounts present in the intestine, which is only the case if drug and lipid amounts were lower than their maximum absorption capacity in the intestine. This might indeed have been the case since fenofibrate is known to be absorbed fast and well [12].

Regarding the biodistribution of lipid excipients (Fig. 7 and 8), more lipid was found in the stomach and the intestine for SBO compared to other the LbDDS containing surfactants and lower lipid levels. A slower gastric emptying rate can be expected from SBO, as lipids are emptied more slowly from a poorly emulsified lipid phase than from a fine oil-in-water emulsion [44]. The lipid SUV in the liver was also higher for LbDDS containing higher triglyceride levels (i.e., SBO and SBO-MAPC) than LbDDS containing lower triglyceride levels (i.e., SNEDDS and SNEDDS-MAPC).

There was a trend that drug uptake in the heart and the liver (Fig. 7) was higher for the SNEDDS as compared to the SUSP and SBO, however, this was not statistically significant. Further, in all 5 formulations, there was no correlation between the distribution

of the drug and the lipid, indicating that they are not co-distributed in the body. One possible explanation might be the high variability between animals, which could be due to the low number of animals used and the inconsistent amount of drug measured in the stomach. For future studies, the inter-subject variability should be reduced by increasing the number of time points and/or animals used. To reduce variations related to gastric emptying, the amount of food and bedding materials in the rat stomach should be reduced by adjusting feeding and housing strategies (e.g., changing food type, circadian rhythm, bedding materials or housing in wire-bottom cages).

3.3.2. Final organ activity measurement and biodistribution

After the final 24 h SPECT/CT imaging time point, the animals were sacrificed and the radioactivity in relevant organs were measured in a calibrated gamma counter to confirm the quantitative imaging data and to provide supplementary information from low activity organs. Organ activity concentrations and organ activities were then calculated the %ID/g and the %ID/organ for different organs, urine and feces (Fig. 9). At 25 h after oral gavage, 32–73% of radiolabeled drug and 16–34% of radiolabeled lipid were found in the stomach content. At the same time point, 0.5–1.6% of radiolabeled drug and 0.4–2.2% of radiolabeled lipid were found in the stomach tissue, and 2–4% of radiolabeled drug and 0.1–0.4% of radiolabeled lipid were found in the whole small intestine (both content and tissue). No significant differences were observed between the five formulations for both ^{123}I-FF and ^{125}I-triolein. Both gamma counter biodistribution analysis and SPECT/CT imaging allow the conclusion that a large amount of drug and lipid excipients remained in the stomach after 24 h post administration. Small differences between the two methods can be attributed to the inhomogeneous distribution of radioactivity in the whole organ. Although the organ tissues and stomach content were thoroughly homogenized, errors might come especially from the small sample volumes used for the gamma counter measurements.

Journal Pre-proof

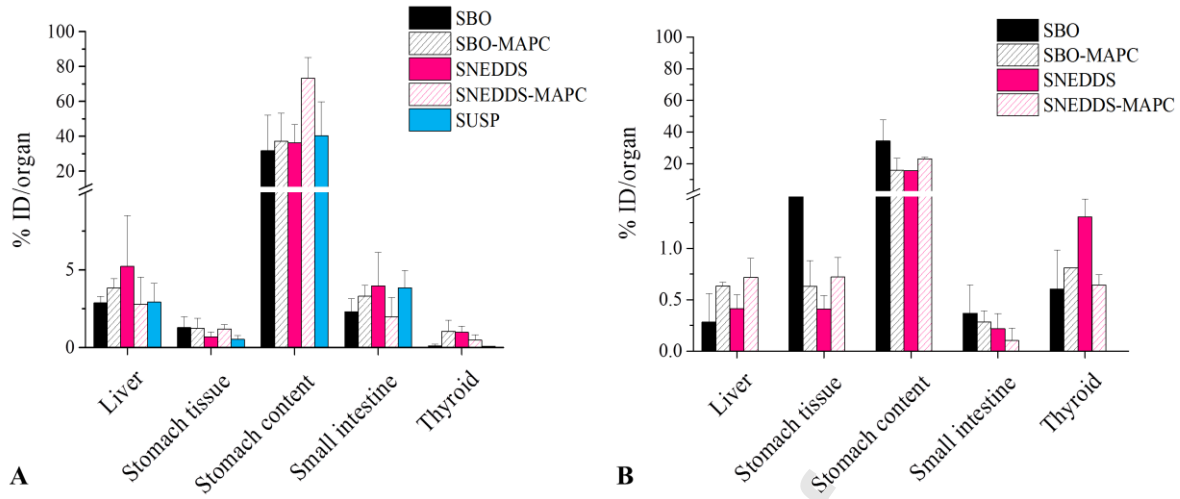

Fig. 9. Organ distribution of (A) radiolabeled drug and (B) radiolabeled lipids measured in the gamma counter 25 h after oral administration and expressed as a percentage of the injected dose. The data are presented as the mean + SD (n = 2–3)

The significant amount of radiolabelled drug found in the gastro-intestinal tract after 24 h can be related to the low absolute bioavailability found in the pharmacokinetic study (i.e., 24 to 35%). This can be either a slow gastric emptying observed in the biodistribution study due to the constantly abundant presence of substances in the rat stomach or the re-ingestion of excreted formulation. In the literature, food was reported to be found in rat stomach after overnight fasting [45]. In addition, during fasting (12 h prior to administration and 6 h post administration) for both the pharmacokinetic and biodistribution studies, the animals were kept in cages with bedding materials mixed with their faeces, which might contain excreted formulation. Hungry animals seem to have a tendency to fill their stomach with these materials, which we found at the 24 h time point during biodistribution in their stomach. Since most radiolabelled drug and lipid was still inside the stomach at that time, it appears that drug and lipid stayed with the bedding materials for a long time.

Besides the stomach and the intestine, radiolabeled drug and lipid were mainly found in the liver, thyroid, blood, faeces and urine by the gamma counter measurements. The distribution of ^{123}I and ^{125}I in the thyroid increased over time indicating that free iodine was released from radiolabelled drug and lipid. Despite a visible radioactivity accumulation in the thyroid (Fig. 6), which increased over the 24 h study period, the maximum radioactivity in the thyroid, i.e., at 24 h post administration, contributed less

than 2% of the total administered radioactivity dose as detected from gamma counter measurements (Fig. 9).

4. CONCLUSION

Results from both two-step *in vitro* lipolysis and dual isotope SPECT/CT imaging studies correlated well with the pharmacokinetic study. Combining these techniques provided a complete explanation of the fate of drug and co-administered excipients with important and precise details on drug solubilisation and biodistribution after oral administration from different formulations. While the aqueous suspension, SUSP, led to the slowest and lowest drug absorption due to low drug solubilisation, SNEDDS with 30% Kolliphor exhibited the fastest absorption of FF and in accordance also displayed a high drug concentration in the aqueous phase during *in vitro* lipolysis. SNEDDS and SBC containing MAPC exhibited enhanced oral bioavailability with prolonged drug absorption profile, which was explained by the enhanced emulsification with drug solubilised in both aqueous and oil phases during lipid digestion. To explain the limited oral bioavailability of LbDDS (less than 34%) despite absorption enhancement, SPECT/CT imaging was used and shown that significant amounts of drug and lipid formulation were found in the animals' stomach even 24 h post administration. The study is a proof-of-concept for the use of SPECT/CT imaging in drug and formulation absorption. A study where the animals are conditioned to become diurnal and/or housed in wire-bottom cages to obtain an empty stomach before administration and avoid re-ingestion of formulation should be performed to reduce artefacts.

Journal Pre-proof

ACKNOWLEDGMENT

Financial support from the University of Copenhagen, the Phospholipid Research Center (Heidelberg, Germany), the Lundbeck Foundation, and the Canadian Foundation for Innovation (CFI, project number 25413) are kindly acknowledged. We are also grateful for the support of technicians and veterinarians at the Department of Pharmacy, University of Copenhagen, Denmark and the Centre for Comparative Medicine, University of British Columbia, Canada.

REFERENCES

[1] S. Stegemann, F. Leveiller, D. Franchi, H. De Jong, H. Lindén, When poor solubility becomes an issue: From early stage to proof of concept, Eur J Pharm Sci, 31 (2007) 249-261.

[2] A. Müllertz, A. Ogbonna, S. Ren, T. Rades, New perspectives on lipid and surfactant based drug delivery systems for oral delivery of poorly soluble drugs, J Pharm Pharmacol, 62 (2010) 1622-1636.

[3] T. Tran, X. Xi, T. Rades, A. Müllertz, Formulation and characterization of self-nanoemulsifying drug delivery systems containing monoacyl phosphatidylcholine, Int J Pharm, 502 (2016) 151-160.

[4] T. Tran, S.D.V.S. Siqueira, H. Amenitsch, A. Müllertz, T. Rades, *In vitro* and *in vivo* performance of monoacyl phospholipid-based self-emulsifying drug delivery systems, J Control Release, 255 (2017) 45-53.

[5] T. Tran, S. Siqueira, H. Amenitsch, T. Rades, A. Mullertz, Monoacyl phosphatidylcholine inhibits the formation of lipid multilamellar structures during *in vitro* lipolysis of self-emulsifying drug delivery systems, Eur J Pharm Sci, 108 (2017) 62-70.

[6] A.T. Larsen, P. Sassene, A. Müllertz, *In vitro* lipolysis models as a tool for the characterization of oral lipid and surfactant based drug delivery systems, Int J Pharm, 417 (2011) 245-255.

[7] J.Ø. Christensen, K. Schultz, E. Mollgaard, H.G. Kristensen, A. Mullertz, Solubilisation of poorly water-soluble drugs during *in vitro* lipolysis of medium-and long-chain triacylglycerols, Eur J Pharm Sci, 23 (2004) 287-296.

[8] A.T. Larsen, A.G. Ohlsson, B. Polentarutti, R.A. Barker, A.R. Phillips, R. Abu-Rmaileh, P.A. Dickinson, B. Abrahamsson, J. Ostergaard, A. Müllertz, Oral bioavailability of cinnarizine in dogs: Relation to SNEDDS droplet size, drug solubility and *in vitro* precipitation, Eur J Pharm Sci, 48 (2013) 339-350.

[9] A. Larsen, R. Holm, M.L. Pedersen, A. Mullertz, Lipid-based formulations for danazol containing a digestible surfactant, Labrafil M2125CS: *in vivo* bioavailability and dynamic *in vitro* lipolysis, Pharm Res, 25 (2008) 2769-2777.

[10] N. Thomas, K. Richter, T.B. Pedersen, R. Holm, A. Müllertz, T. Rades, *In vitro* lipolysis data does not adequately predict the *in vivo* performance of lipid-based drug delivery systems containing fenofibrate, AAPS J, 16 (2014) 539-549.

Journal Pre-proof

[11] T.T. Do, M. Van Speybroeck, R. Mols, P. Annaert, J. Martens, J. Van Humbeeck, J. Vermant, P. Augustijns, G. Van den Mooter, The conflict between *in vitro* release studies in human biorelevant media and the *in vivo* exposure in rats of the lipophilic compound fenofibrate, Int J Pharm, 414 (2011) 118-124.

[12] M.F. Crum, N.L. Trevaskis, H.D. Williams, C.W. Pouton, C.J.H. Porter, A new *in vitro* lipid digestion – *in vivo* absorption model to evaluate the mechanisms of drug absorption from lipid-based formulations, Pharm Res, 33 (2015) 970-982.

[13] M.H. Michaelsen, K.M. Wasan, O. Sivak, A. Müllertz, T. Rades, The effect of digestion and drug load on halofantrine absorption from self-nanoemulsifying drug delivery system (SNEDDS), AAPS J, 18 (2016) 180-186.

[14] R. Berthelsen, R. Holm, J. Jacobsen, J. Kristensen, B. Abrahamsson, A. Müllertz, Kolliphor surfactants affect solubilization and bioavailability of fenofibrate. studies of *in vitro* digestion and absorption in rats, Mol Pharm, 12 (2015) 1062-1071.

[15] W. Weitschies, C.G. Wilson, *In vivo* imaging of drug delivery systems in the gastrointestinal tract, Int J Pharm, 417 (2011) 216-226.

[16] C.M. Gomes, A.J. Abrunhosa, P. Ramos, F.K. Pauwels, Molecular imaging with SPECT as a tool for drug development, Adv Drug Deliv Rev, 63 (2011) 547-554.

[17] R. Misri, K. Saatchi, U.O. Häfeli, Nanoprobes for hybrid SPECT/MR molecular imaging, Nanomedicine (Lond), 7 (2012) 719-733.

[18] K. Saatchi, P. Soema, N. Geider, R. Misri, K. McPhee, J.H. Baker, S.A. Reinsberg, D.E. Brooks, U.O. Häfeli, Hyperbranched polyglycerols as trimodal imaging agents: design, biocompatibility, and tumor uptake, Bioconjug Chem, 23 (2012) 372-381.

[19] K. Saatchi, U.O. Häfeli, Radiolabeling of biodegradable polymeric microspheres with $[^{99m}TC(CO)_3]+$ and *in vivo* biodistribution evaluation using MicroSPECT/CT imaging, Bioconjug Chem, 20 (2009) 1209-1217.

[20] R. Misri, K. Saatchi, S.S. Ng, U. Kumar, U.O. Häfeli, Evaluation of 111In labeled antibodies for SPECT imaging of mesothelin expressing tumors, Nucl Med Biol, 38 (2011) 885-896.

[21] H.D. Williams, P. Sassene, K. Kleberg, J.C. Bakala-N'Goma, M. Calderone, V. Jannin, A. Igonin, A. Partheil, D. Marchaud, E. Jule, Toward the establishment of standardized *in vitro* tests for lipid-based formulations, part 1: method parameterization and comparison of *in vitro* digestion profiles across a range of representative formulations, J Pharm Sci, 101 (2012) 3360-3380.

Journal Pre-proof

[22] M.C. Michalski, C. Genot, C. Gayet, C. Lopez, F. Fine, F. Joffre, J.-L. Vendeuvre, J. Bouvier, J.-M. Chardigny, K. Raynal-Ljutovac, Multiscale structures of lipids in foods as parameters affecting fatty acid bioavailability and lipid metabolism, Progress in lipid research, 52 (2013) 354-373.

[23] D.N. Lorenz, Gastric emptying of milk in rat pups, Am J Physiol, 248 (1985) R732-738.

[24] J. Jordi, F. Verrey, T.A. Lutz, Simultaneous assessment of gastric emptying and secretion in rats by a novel computed tomography-based method, Am J Physiol, 306 (2014) G173-G182.

[25] R. Holm, A. Müllertz, H. Mu, Bile salts and their importance for drug absorption, Int J Pharm, 453 (2013) 44-55.

[26] R. Coleman, S. Iqbal, P.P. Godfrey, D. Billington, Membranes and bile formation. Composition of several mammalian biles and their membrane-damaging properties, Biochem J, 178 (1979) 201-208.

[27] M. Hagio, M. Matsumoto, M. Fukushima, H. Hara, S. Ishizuka, Improved analysis of bile acids in tissues and intestinal contents of rats using LC/ESI-MS, J Lipid Res, 50 (2009) 173-180.

[28] T.T. Kararli, Comparison of the gastrointestinal anatomy, physiology, and biochemistry of humans and commonly used laboratory animals, Biopharm Drug Dispos 16 (1995) 351-380.

[29] P. Sassene, M. Michaelsen, M. Mosgaard, M. Jensen, E. Van Den Broek, K. Wasan, H. Mu, T. Rades, A. Müllertz, *In vivo* precipitation of poorly soluble drugs from lipid-based drug delivery systems, Mol Pharm, 13 (2016) 3417-3426.

[30] M.U. Anby, T.-H. Nguyen, Y.Y. Yeap, O.M. Feeney, H.D. Williams, H. Benameur, C.W. Pouton, C.J. Porter, An *in vitro* digestion test that reflects rat intestinal conditions to probe the importance of formulation digestion vs first pass metabolism in danazol bioavailability from lipid based formulations, Mol Pharm, 11 (2014) 4069-4083.

[31] S. Breyer, A. Semmler, T. Miller, A. Hill, S. Geissler, U. Haberkorn, W. Mier, Radioiodinated dechloro-4-iodofenofibrate: a hydrophobic model drug for molecular imaging studies, Int J Pharm, 431 (2012) 78-83.

[32] M. Lubran, J.D. Pearson, A screening test for steatorrhoea using ^{131}I-labelled triolein, J Clin Pathol, 11 (1958) 165-169.

[33] F. van der Have, B. Vastenhouw, R.M. Ramakers, W. Branderhorst, J.O. Krah, C. Ji, S.G. Staelens, F.J. Beekman, U-SPECT-II: An ultra-high-resolution device for molecular small-animal imaging, J Nucl Med, 50 (2009) 599-605.

Journal Pre-proof

[34] W. Branderhorst, B. Vastenhouw, F.J. Beekman, Pixel-based subsets for rapid multi-pinhole SPECT reconstruction, Phys Med Biol, 55 (2010) 2023-2034.

[35] C. Wu, J.R. de Jong, H.A. Gratama van Andel, F. van der Have, B. Vastenhouw, P. Laverman, O.C. Boerman, R.A. Dierckx, F.J. Beekman, Quantitative multi-pinhole small-animal SPECT: Uniform versus non-uniform Chang attenuation correction, Phys Med Biol, 56 (2011) N183-193.

[36] K. Ogawa, Y. Harata, T. Ichihara, A. Kubo, S. Hashimoto, A practical method for position-dependent compton-scatter correction in single photon emission CT, IEEE Trans Med Imaging, 10 (1991) 408-412.

[37] C. Wu, F. van der Have, B. Vastenhouw, R.A.J.O. Dierckx, A.M.J. Paans, F.J. Beekman, Absolute quantitative total-body small-animal SPECT with focusing pinholes, Eur J Nucl Med Mol Imaging, 37 (2010) 2127-2135.

[38] Z.P. Nosrati, P. Esquinas, C. Rodriguez-Rodriguez, T. Tran, T. Esposito, K. Saatchi, U.O. Häfeli, Simultaneous SPECT imaging of I-125 and I-123, a practical approach to assessing a drug and its carrier at the same time with preclinical dual imaging, (In preparation).

[39] N. Borkar, Oral delivery of fenofibrate-loaded lipid matrix particles, Master Thesis, Department of Pharmacy, University of Copenhagen, Copenhagen, Denmark, 2012.

[40] D.B. Miller, J.D. Spence, Clinical pharmacokinetics of fibric acid derivatives (fibrates), Clin Pharmacokinet, 34 (1998) 155-162.

[41] M.J. Chapman, Pharmacology of fenofibrate, Am J Med, 83 (1987) 21-25.

[42] C.M. Lo, P. Tso, 4 - Physicochemical basis of the digestion and absorption of triacylglycerol, in: Designing Functional Foods, Woodhead Publishing, 2009, pp. 94-125.

[43] S. Lee, J. Gregor, S.J. Kennel, D.R. Osborne, J. Wall, GATE Validation of standard dual energy corrections in small animal SPECT-CT, PLOS ONE, 10 (2015) e0122780.

[44] M.I. Friedman, I. Ramirez, M.G. Tordoff, Gastric emptying of ingested fat emulsion in rats: implications for studies of fat-induced satiety, Am J Physiol, 270 (1996) R688-692.

[45] P. Jeffrey, M. Burrows, A. Bye, Does the rat have an empty stomach after an overnight fast?, Lab Anim, 21 (1987) 330-334.

Graphical abstract: